BIOCHEMISTRY
including biophysical chemistry & molecular biology

Article

pubs.acs.org/biochemistry

Mechanism for N_2O Generation in Bacterial Nitric Oxide Reductase: A Quantum Chemical Study

Margareta R. A. Blomberg* and Per E. M. Siegbahn

Department of Physics, AlbaNova university center, and Department of Biochemistry and Biophysics, Arrhenius Laboratory, Stockholm University, SE-106 91 Stockholm, Sweden

Supporting Information

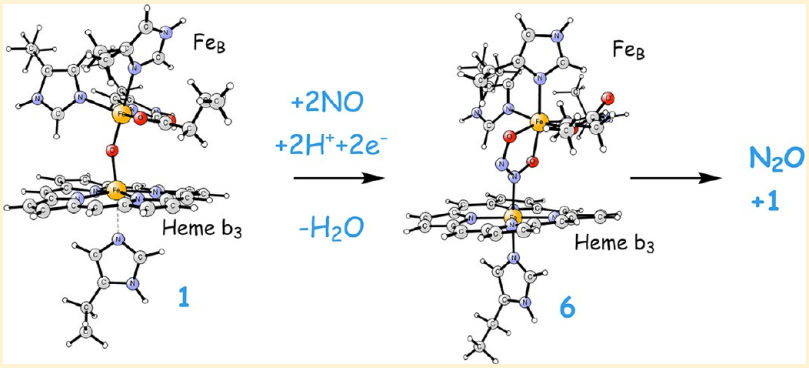

ABSTRACT: The catalytic mechanism of reduction of NO to N_2O in the bacterial enzyme nitric oxide reductase has been investigated using hybrid density functional theory and a model of the binuclear center (BNC) based on the newly determined crystal structure. The calculations strongly suggest a so-called cis:b_3 mechanism, while the commonly suggested trans mechanism is found to be energetically unfavorable. The mechanism suggested here involves a stable cis-hyponitrite, and it is shown that from this intermediate one N−O bond can be cleaved without the transfer of a proton or an electron into the binuclear active site, in agreement with experimental observations. The fully oxidized intermediate in the catalytic cycle and the resting form of the enzyme are suggested to have an oxo-bridged BNC with two high-spin ferric irons antiferromagnetically coupled. Both steps of reduction of the BNC after N_2O formation are found to be pH-dependent, also in agreement with experiment. Finally, it is found that the oxo bridge in the oxidized BNC can react with NO to give nitrite, which explains the experimental observations that the fully oxidized enzyme reacts with NO, and most likely also the observed substrate inhibition at higher NO concentrations.

The membrane-integrated enzyme nitric oxide reductase (NOR) catalyzes the reduction of nitric oxide (NO) to nitrous oxide (N_2O) as one of the steps in the denitrification pathway, transforming nitrite (NO_3^-) to dinitrogen (N_2). The NOR enzyme belongs to the heme-copper oxidase superfamily, together with cytochrome *c* oxidase (CcO), the terminal enzyme in the aerobic respiratory chain. In both NOR and CcO, the catalytically active site is a binuclear center with a heme group and a non-heme metal ion, which is copper (Cu_B) in CcO and iron (Fe_B) in NOR. Until recently, the crystal structure of NOR was not known, and the organization of the active site could only be guessed on the basis of the homology with CcO, for which crystal structures have been known for several years for different species. On the basis of such a tentative structure of the active site and different types of experimental and computational information, possible mechanisms for the catalytic reaction have been suggested.[1−9] In 2010, the crystal structure was finally determined for the bacterial cNOR of *Pseudomonas aeruginosa* at 2.7 Å resolution,[10] with an active site as shown in Figure 1A. With the crystal structure at hand, it is possible to construct reliable models for quantum chemical calculations, and the different suggestions for the catalytic mechanism can be evaluated on the basis of energetics. In this study, we show that only a so-called cis:b_3 mechanism is energetically feasible, and the suggested alternative trans mechanisms most likely have to be rejected as energetically unfavorable.

The chemical reaction occurring in NOR is a two-electron reduction of nitric oxide to nitrous oxide and water, which can be written

$$2NO + 2H^+ + 2e^- \rightarrow N_2O + H_2O \quad (1)$$

In cNOR, the electrons are delivered by reduced cytochrome *c* from the outside of the enzyme, and the protons are taken up from bulk water. In contrast to the situation in CcO, there is no electrochemical gradient built up over the membrane in NOR, implying that the electrons and the protons are taken from the

Received: April 17, 2012
Revised: May 30, 2012
Published: June 8, 2012

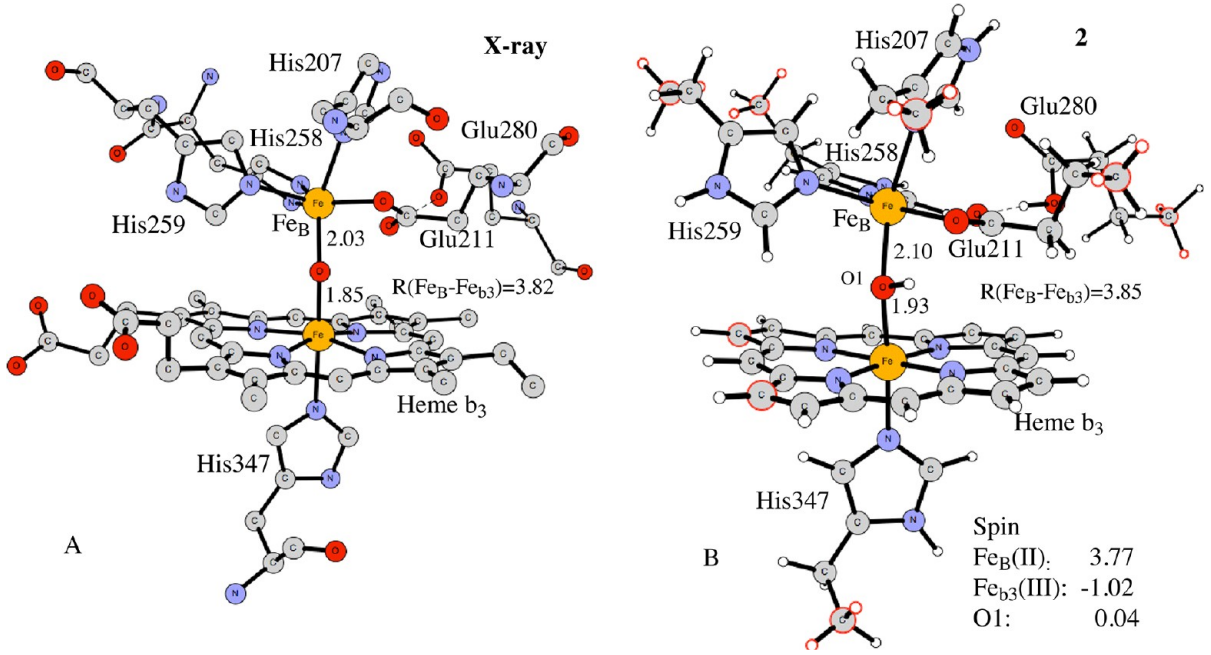

Figure 1. (A) X-ray structure of the binuclear center in NOR from *P. aeruginosa*.[10] (B) Model used in the calculations, showing the optimized structure of the one-electron-reduced and protonated state (**2**, quartet). The atoms with red circles are fixed from the X-ray structure during the geometry optimization of all structures. A few interatomic distances are given (in angstroms), as well as the most important spin populations.

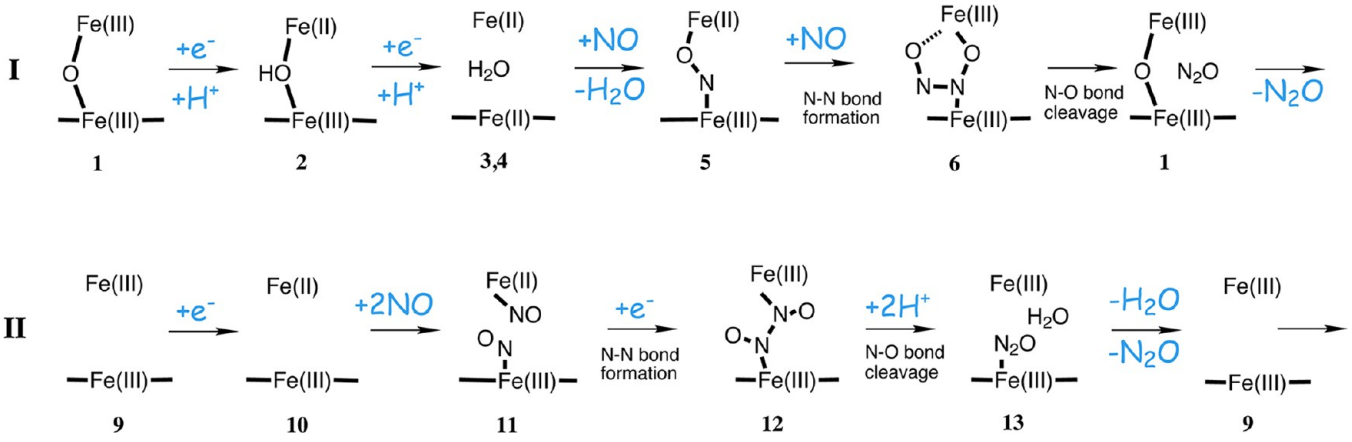

Figure 2. Two suggested mechanisms for the catalytic reaction starting from the oxidized binuclear center of NOR. Mechanism I is an example of a cis:b_3 mechanism and mechanism II an example of a trans mechanism.

same side of the membrane.[11,12] Similar to CcO, there are four redox active metal centers in NOR, which in cNOR consists of three heme groups and one non-heme iron, Fe_B. As mentioned above, one of the heme groups, a heme b_3, and Fe_B constitute the catalytically active binuclear center (BNC). The two other heme groups, heme c and heme b, also termed low-spin hemes, are used to transport the electrons from cytochrome *c* to the BNC. Because there are four redox centers available, and only two electrons are needed for the formation of one molecule of N_2O, the fully reduced enzyme can perform two turnovers, which is used in experiments with this form of the enzyme. The catalytic reaction thus occurs in several steps, involving the formation of an N−N bond, cleavage of an N−O bond, and two steps each of electron and proton transfer, which in principle can be organized in several ways, with respect to both the order of the individual steps and the structure of the intermediates formed. In Figure 2, two different mechanisms are sketched; mechanism I is an example of a so-called cis:b_3 mechanism, where the two NO molecules bind in a cis manner to the heme b_3 iron, and mechanism II is an example of a so-called trans mechanism in which the two NO molecules bind in a trans manner to the two iron ions in the BNC. A cis:b_3 mechanism has previously been suggested for NOR on the basis of a computational investigation using tentative models of the BNC, performed before the crystal structure was known.[7] Also, in analogy with results obtained for NO reduction in bacterial cytochrome *c* oxidase,[4,6] cis:b_3 mechanisms have been identified as a possibility for NOR.[8] There are also suggestions for cis mechanisms in which NO binds to Fe_B (see, for example, ref 8 and references cited therein). Trans mechanisms for NO reduction in NOR have been suggested by several authors on the basis of different types of experimental data.[1−3,5,9,13] The specific form of the trans mechanism illustrated in Figure 2 is built on the mechanism sketched in ref 13.

A large amount of experimental data has been collected to understand the properties and the mechanisms of NOR. Before

dx.doi.org/10.1021/bi300496e | *Biochemistry* 2012, 51, 5173−5186

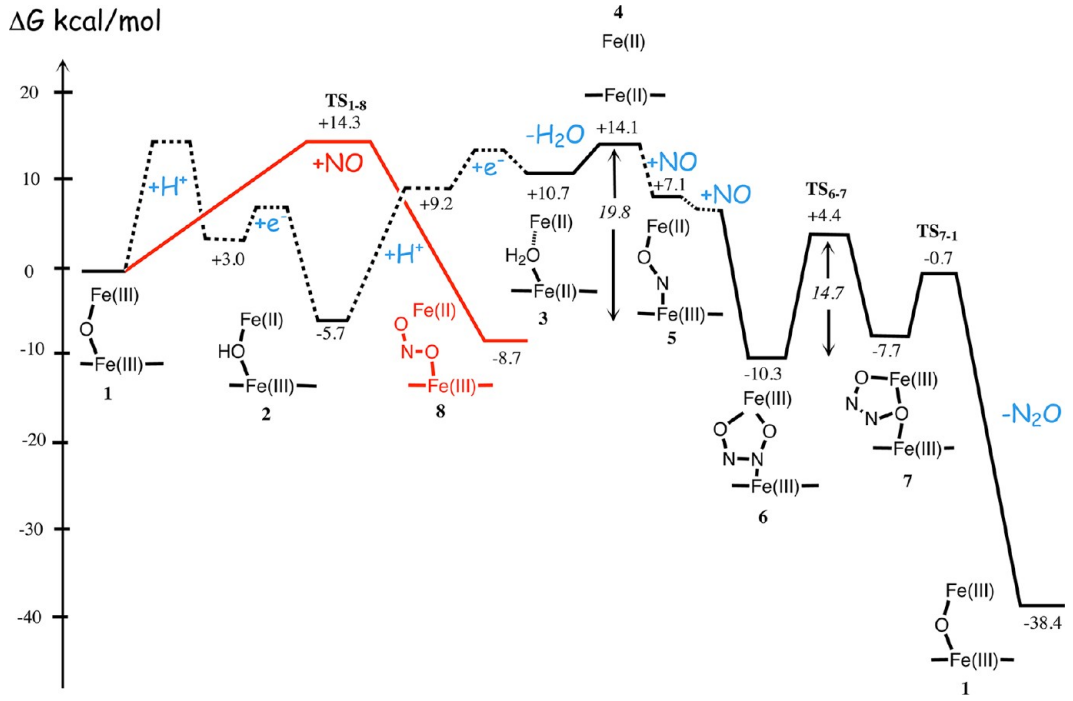

Figure 3. Calculated free energy profile for mechanism I starting from the oxidized binuclear center of NOR (black curve). The red curve corresponds to a side reaction between oxidized NOR and NO leading to nitrite (see the text).

the X-ray structure of the enzyme was published, several experimental studies using different spectroscopic techniques were conducted to elucidate the structural properties of the active site, in particular of the BNC itself.[1−3,5,14] This type of study can still provide important information about the stuctural details of intermediates at different reduction levels. In other types of studies, the redox properties of the cofactors have been studied, to shed light on the ordering of the electron and proton transfer steps in relation to the substrate-binding, bond-forming, and bond-cleavage steps.[15,16] Another set of experiments were concerned with the transfer of the protons to the active site.[17,18] This is of particular interest because it has been found that in contrast to the homologous enzyme CcO, the reaction in NOR is nonelectrogenic, and no protons are pumped,[11,12] although the NO reduction in NOR has an exergonicity similar to that of the O_2 reduction in CcO. The reasons for this difference are still under debate. The scope of this study is limited to the investigation of the catalytic reaction mechanism at the BNC, including the identification of the stages for the transfer of protons and electrons to the BNC. Some of the experimental data obtained can be understood on the basis of the computational findings, as will be discussed below. One of the more intriguing experimental observations is substrate inhibition, i.e., a decreased catalytic activity for higher NO concentrations has been observed.[1,19] Apart from suggesting a likely catalytic mechanism, the computational results present a plausible new explanation for the substrate inhibition.

As mentioned above, the BNC of NOR is quite similar to the BNC of CcO. The main difference is the coordination of the non-heme metal ion, where Fe_B in NOR, apart from the three histidines present also as ligands to Cu_B in CcO, has a glutamate (Glu211) in the first coordination shell.[10] This was actually predicted in the early computational study where it was shown that a negatively charged ligand at Fe_B, such as Glu211, was needed to give an energetically feasible mechanism.[7] Glu211 has also been shown to be essential for enzyme activity[20] and has been proposed to be a possible ligand of Fe_B, even if it was placed too far from Fe_B in the model structure constructed by Zumft in 2005.[21] The model of the BNC used in this study is shown in Figure 1B. One difference compared to the model used in the previous computational study[7] is that in the previous study a water molecule was added as a ligand to Fe_B to yield an octahedral coordination, which was not done in this study. In the crystal structure, there is no such water ligand, and in this study, we found that adding a water ligand to Fe_B is endergonic (see below). Another difference is that in this study, coordinates for certain atoms are fixed to keep the structure similar to the crystal structure, which obviously could not be done in the previous study. Minor differences are that slightly larger models for the amino acids are used in our study and that one neutral second-shell glutamic acid ligand (Glu280) is now included. The main conclusion, that the catalytic reaction mechanism most likely is of the cis-heme b_3 type, is the same in the old and new studies. However, there are several important differences making this study more informative, and also more reliable, as will be discussed below. The most important results from this study are summarized in the free energy diagram in Figure 3, and the most likely catalytic mechanism emanating from those results is sketched as mechanism I in Figure 2.

■ COMPUTATIONAL DETAILS

A model of the BNC was constructed starting from the crystal structure[10] (see Figure 1). The model contains heme b_3, modeled as an unsubstituted porphyrin, and its proximal His347, and Fe_B with its first-shell ligands, His258, His259, His207, and Glu211, together with one second-shell ligand, Glu280. The latter is included because the crystal structure shows that it forms a hydrogen bond to the unprotonated Glu211, and it could be expected to have some effects on the flexibility of the Fe_B coordination. It can be noted that there is

dx.doi.org/10.1021/bi300496e | Biochemistry 2012, 51, 5173−5186

no choice for the protonation state of Glu280, because the hydrogen bonding to Glu211 forces Glu280 to be protonated. In the model used, the proton is free to move between Glu211 and Glu280, but as it turns out, it stays on Glu280; the omission of Glu280 from the model is expected to have an only weak effect on the results. In fact, also for the determination of one of the transition states ($\mathbf{TS}_{6-7}$), a smaller model without Glu280 was used, yielding a barrier height within 2 kcal/mol of the value obtained for the main model. Furthermore, in the crystal structure, Fe_B is essentially five-coordinate (distorted trigonal bipyramidal), because Glu211 is mainly coordinating with only one of its oxygens. With a ferric iron, a regular octahedral coordination with six ligands could be expected, and therefore, the addition of a water molecule as a ligand to Fe_B was tested in those cases. It was found, however, that in all cases the water molecule was less bound to Fe_B than to bulk water, and therefore, in the results reported here, no such extra water ligand is included. All amino acids are truncated at the α-carbon, which is fixed to the X-ray coordinates during geometry optimizations to maintain some of the constraints from the surrounding protein. The peptide bonds are replaced by C−H bonds, with the hydrogen atoms fixed. The two carbon atoms on the porphyrin ring where the propionate groups would be linked are also fixed. The model is depicted in Figure 1B, where the fixed atoms are marked by red circles. The model has ∼130 atoms, with the exact number depending on the stage of the reaction. The total charge of the model is +1 in most states considered, with the exception of a few states in which proton transfer but not electron transfer has occurred. The non-heme iron is always in a high-spin state, while the heme iron is mostly in a low-spin state, with some exceptions discussed in the text. In most cases, spin coupling between the two iron ions in the BNC is weak and the energy difference between ferromagnetic and antiferromagnetic coupling is small. In only one case, in the resting state with an oxo bridge, the splitting between the ferromagnetic and antiferromagnetic coupled states is large enough to cause the introduction of a broken symmetry correction[22] (see below).

Quantum mechanical calculations were performed on the BNC model employing the hybrid density functional B3LYP.[23] There are indications that the reparametrized B3LYP* functional, which uses 15% Hartree−Fock exchange as compared to the 20% exchange used in the original functional, gives a better description of relative energies in transition metal-containing systems.[24] In particular, the discrepancy in calculated relative energies obtained with the two functionals, B3LYP and B3LYP*, gives an indication of the reliability of the results. Therefore, both the B3LYP functional and the B3LYP* functional were used to calculate the final relative energies. All structures were fully optimized, except for some atoms fixed from the crystal structure as discussed above, using the B3LYP functional and the double-ζ basis set labeled lacvp in Jaguar.[25] Single-point calculations were performed in the optimized structures using the large cc-pvtz(-f) basis set plus lacv3p+ for the iron ions with both B3LYP and B3LYP* functionals. Single-point dispersion effects are included using the empirical formula by Grimme,[26] because it has been shown that the lack of dispersion in DFT theory may lead to large errors when molecules are forced closer to each other.[26,27] Solvent effects from the surrounding protein were included using the self-consistent reaction field (SCRF) approach as implemented in Jaguar with a dielectric constant of 4, in accordance with previous work.[28] The dielectric calculations were performed for the optimized structures using the B3LYP functional and the lacvp* basis set, which has polarization functions on all second-row atoms. The solvent effects on relative energies are quite small in this study, typically not more than 1−2 kcal/mol, comparing systems with the same charge. For the calculated proton and electron affinities, the effects are obviously much larger (see below). Jaguar version 7.6[25] was used in all calculations described so far.

Several benchmark tests of the accuracy of the B3LYP functional have been performed,[29] and on the basis of those results, an average error of 3−5 kcal/mol is expected for the computed relative energies for transition metal-containing systems.[30]

For the bond formation and bond cleavage reaction steps, approximate transition states were determined by constrained optimization at different bond distances. The structures of the approximate transition states obtained in this way were used in full transition state optimizations with an explicitly calculated Hessian matrix, i.e., second derivatives of the energy with respect to the nuclear coordinates. The calculation of the Hessian matrices as well as the full transition state optimizations were performed using the Gaussian 03 package[31] at the same level of calculation as the rest of the geometry optimizations [B3LYP/lacvp (imported from Jaguar into Gaussian)]. The Hessians were calculated for the optimized minima as well, yielding zero-point corrections for all relative energies. Because of the fixed coordinates in the geometry optimizations, entropy effects would not be reliable and could not be taken from the Hessian calculations (see below).

To obtain an energy diagram for a full catalytic cycle of NOR, one must calculate the energetics of the reduction steps. This means that the redox potentials of the active site have to be compared to the redox potential of the electron donor, and the pK_a values of the active site have to be compared to the pK_a value of the proton donor, i.e., bulk water. Because it is difficult to calculate accurate absolute redox potentials and pK_a values, a different procedure has been developed and used in several similar cases.[7,32−35] Using quantum chemical methods to calculate redox potentials and pK_a values corresponds to the calculation of electron and proton affinities, properties that are strongly dependent on the surroundings because the charge is changed. Therefore, the SCRF approach, which works very well for calculation of relative energies with a constant charge, is not sufficiently accurate to give absolute electron and proton affinities. However, relative redox potentials and pK_a values for the same site (such as the BNC) can be calculated with much higher accuracy, because the surroundings are the same in all steps. By adjusting the calculated energetics of the entire catalytic cycle to the total reaction energy obtained from experimental reduction potentials, we can obtain accurate energy diagrams, where every second step in the reduction procedure is determined. Via the introduction of one parameter, the relative electron and proton affinities can be used to describe the individual steps of transfer of electrons and protons to the BNC.

As mentioned above, the entropy changes during the reaction, which are needed to obtain free energies, cannot be obtained from the calculated Hessians because of the fixing of certain coordinates. The entropy changes within the BNC itself can rather safely be assumed to be small and therefore neglected. The main entropy changes occur when molecules enter or leave the system, and these have to be estimated in some way. For the gaseous molecules (NO and N_2O), it is

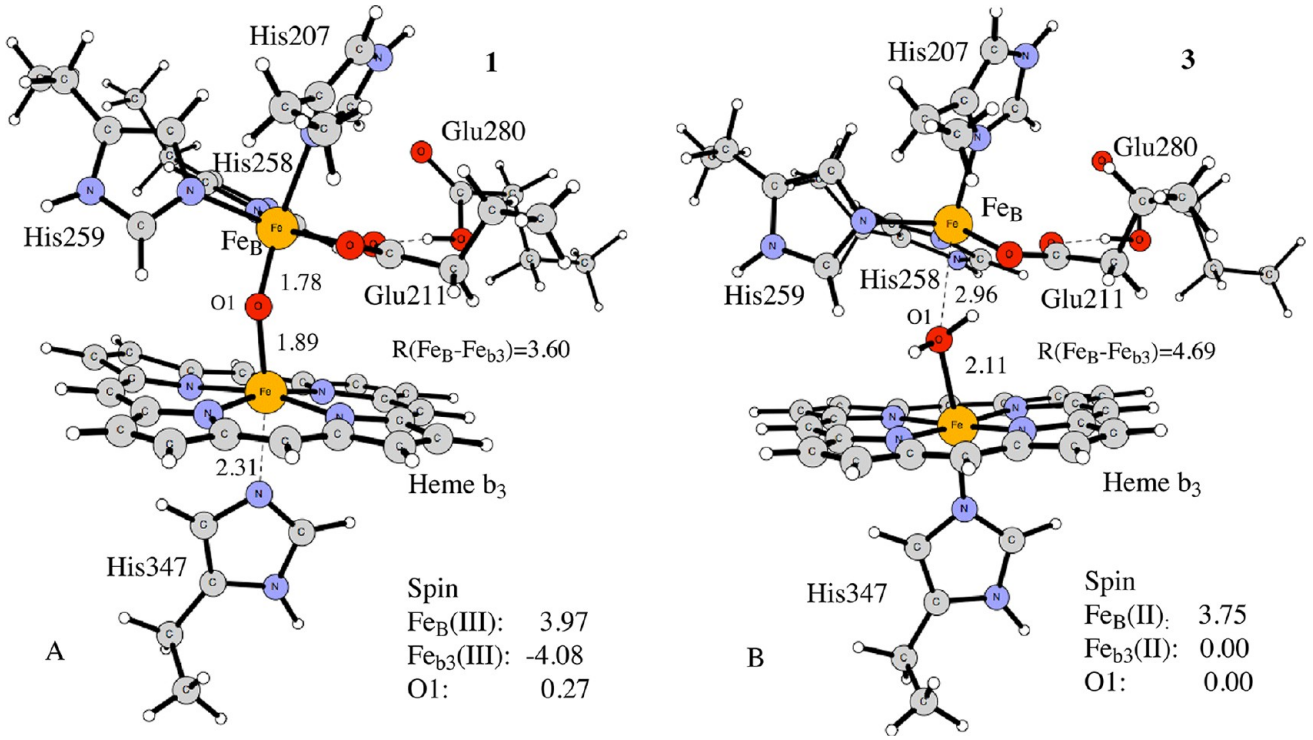

Figure 4. Optimized structures of (A) the oxidized binuclear center (**1**, singlet) and (B) the two-electron-reduced binuclear center with one water bound (**3**, quintet). A few interatomic distances are given (in angstroms), as well as the most important spin populations.

assumed that the entropy lost (on binding) or gained (when released) is equal to the translational entropy for the free molecule (10.8 kcal/mol for NO and 11.1 kcal/mol for N_2O at room temperature). For the binding of a water molecule to bulk water, a standard value of 14 kcal/mol is used.

The relative energies reported below are termed free energy values, with entropy effects estimated as described in the previous paragraph. The enthalpy values are obtained from the large basis set calculations using the B3LYP* functional, including zero-point effects, dispersion, and solvent effects. If the B3LYP results are used instead of the B3LYP* results, a similar picture is obtained and most relative energy values differ by <1 kcal/mol. Somewhat larger differences between the functionals (2−4 kcal/mol) are obtained in a few situations, involving the relative reduction potentials of the BNC, the binding of NO or a water molecule to the reduced BNC, and the relative energies between different spin couplings on the heme iron.

■ RESULTS AND DISCUSSION

Using the model of the BNC and the procedures described above, the structures and the energetics of all intermediates and transition states of the entire catalytic cycle were determined. In this section, the results are presented and discussed. In the first subsection, the experimental information explicitly used will be discussed, i.e., the structure of the BNC and the reduction potentials used to obtain the overall exergonicity. In the next three subsections, different segments of the catalytic cycle will be discussed, i.e., the reduction steps, N−N bond formation, and N−O bond cleavage. After that, the energetics of possible trans mechanisms will be presented in one subsection. Some experimental results will be discussed in light of our calculations, and a possible explanation of the observed substrate inhibition will be presented in the following subsections. Finally, possible modifications of the suggested mechanism will be discussed.

Experimental Information: Overall Energy and Structure of the BNC. As mentioned above, to obtain the overall exergonicity of the catalytic cycle, we used experimental reduction potentials. The immediate electron donor to the BNC is heme b, with a midpoint reduction potential of 0.345 V.[15] It is furthermore known that the potential for reduction of two molecules of nitric oxide to nitrous oxide and water is 1.177 V relative to the standard hydrogen electrode (SHE) at pH 7.0. This gives an experimental exergonicity of 38.4 kcal/mol for the reaction in eq 1 when the electrons are delivered by heme b. Using the calculated free energy for the chemistry in eq 1, the cost of each reduction step (transfer of one electron from heme b and one proton from the bulk) can be set to yield a total exergonicity of 38.4 kcal/mol for reaction 1. This determines the energetics for each of the two reduction steps in the catalytic cycle. Via the introduction of one parameter, the energetics of the individual proton and electron transfer steps can also be calculated (see the next subsection).

The BNC model used in the calculations is described in Computational Details, and it is based on the crystal structure reported for the bacterial cNOR of *P. aeruginosa* at 2.7 Å resolution.[10] The crystal was prepared in a purified ferric resting form,[10] and the BNC was found to have a bridging oxide ligand as expected for the fully oxidized resting state. However, the calculated distances indicate that the BNC in the crystal structure most probably is a one-electron-reduced form with Fe_B in the ferrous state. In the X-ray structure, shown in Figure 1A, the distances from the bridging oxygen to Fe_B and the heme iron are 2.03 and 1.85 Å, respectively. In the singly reduced (and protonated) state, shown in Figure 1B, the distances are 2.10 and 1.93 Å, respectively, i.e., reasonably similar to those of the crystal structure, while they are quite

dx.doi.org/10.1021/bi300496e | *Biochemistry* 2012, 51, 5173−5186

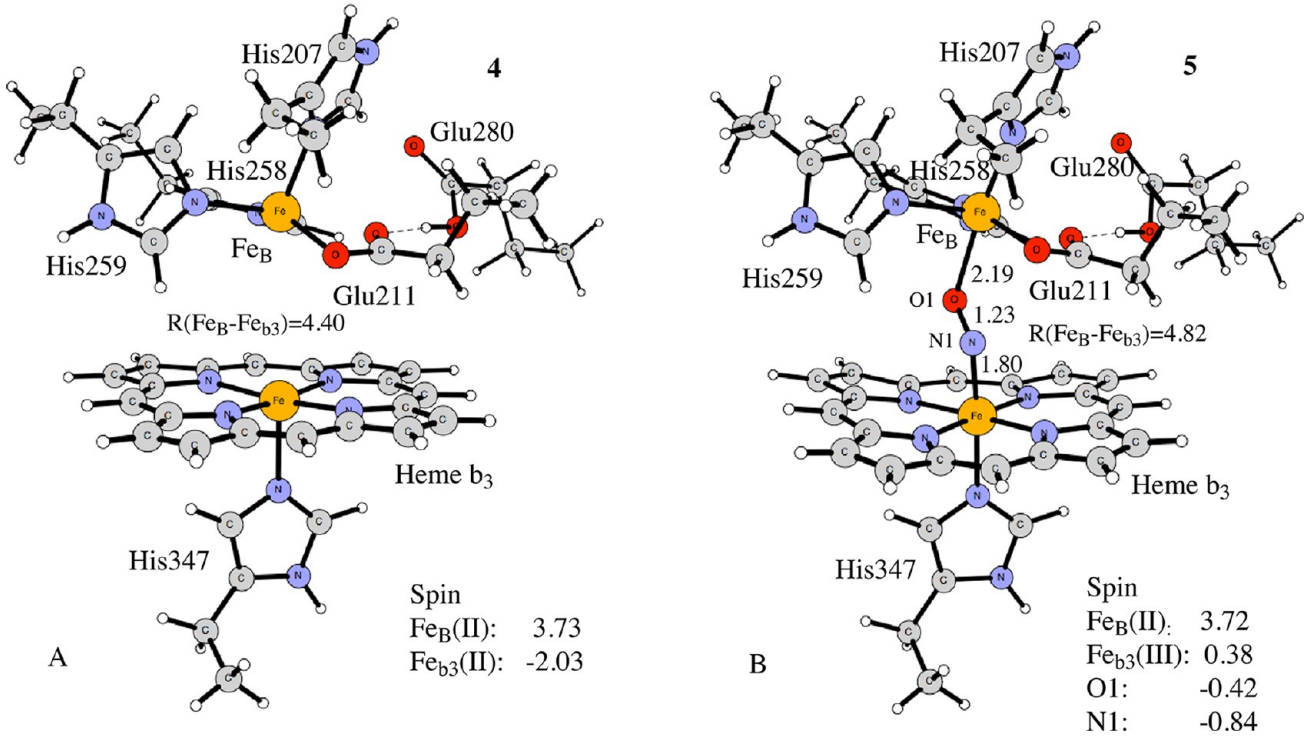

Figure 5. Optimized structures of (A) the two-electron-reduced binuclear center without ligand (**4**, triplet) and (B) the two-electron-reduced binuclear center with one NO bound (**5**, quartet). A few interatomic distances are given (in angstroms), as well as the most important spin populations.

different in the fully oxidized state [1.78 and 1.89 Å, respectively (shown in Figure 4A)]. In particular, the Fe−Fe distance is 3.82 Å in the crystal structure, 3.85 Å in the optimized singly reduced state, and only 3.60 Å in the optimized fully oxidized state. Thus, the structure of the singly reduced state agrees better with the crystal structure than that of the resting oxidized state. Such a reduction of a crystal is known to be a rather common consequence of X-ray irradiation.[36]

Reduction Steps. Experimental observations show that the BNC in the resting oxidized state of NOR is EPR-silent, which is interpreted to be due to an antiferromagnetic coupling of two high-spin ferric irons via an oxo bridge.[2] Furthermore, resonance Raman studies of the oxidized enzyme indicate that the high-spin heme b_3 is pentacoordinate.[2] In the calculations on the oxidized BNC with an oxo bridge (**1**), two states are found to be close in energy, a singlet state involving two high-spin ferric iron ions and a quintet state involving a high-spin Fe_B and a low-spin heme b_3, in both cases with antiferromagnetic coupling. The singlet state, with a high-spin heme b_3, has a long Fe−N distance of 2.31 Å between the heme iron and the proximal His347, while with a low-spin heme b_3, the corresponding distance is only 2.03 Å. Thus, the singlet state, with an optimized geometry shown in Figure 4A, together with the most important spin populations, fits well into the experimental observations for both an EPR silent BNC and a five-coordinate heme b_3. Also, Fe_B is essentially five-coordinate (distorted trigonal bipyramidal), because Glu211 is mainly coordinating with only one of its oxygens. A regular octahedral coordination with six ligands was tried via addition of a water ligand to the ferric Fe_B, but the water ligand was found to be unbound relative to bulk water and was therefore not included. Using the B3LYP functional, the singlet state (with a high-spin heme iron) is the ground state, with the quintet state (with a low-spin heme iron) 3.8 kcal/mol higher, while the B3LYP* functional gives two essentially isoergonic states (the singlet state 0.4 kcal/mol higher than the quintet state). For the singlet state (involving high-spin heme b_3), a broken symmetry correction[22] (∼1.5 kcal/mol) is applied, while when the low-spin heme b_3 is involved, antiferromagnetic coupling and ferromagnetic coupling yield essentially the same energy and no correction is needed. It can be noted that the amount of exact exchange has little effect on the spin coupling between two metal centers; in particular, the splitting between antiferromagnetic and ferromagnetic coupling between the high- and low-spin irons is very close to zero (<0.3 kcal/mol) for the B3LYP and B3LYP* functionals. In the energy diagram in Figure 3 and in the following discussion, the singlet coupled oxidized state is used as the reference state.

Adding a proton leads to the oxidized state with a hydroxo ligand, which has a low-spin heme b_3 and a high-spin Fe_B, with antiferromagnetic and ferromagnetic coupling being essentially degenerate. The experimental information indicates that the resting state of the enzyme is the oxo-bridged state discussed in the preceding paragraph, which means that the state with a hydroxo bridge should be at least 3 kcal/mol higher in energy (yielding an occupancy of at most 1%). This information, together with the calculated proton affinity of the oxo state, can be used to determine the parameter for the proton cost discussed above, making it possible to include the individual steps of proton and electron transfer in the energy diagram. The transfer of the first electron gives the singly reduced state (**2**) shown in Figure 1B, here suggested to be the state present in the crystal structure. The ground state has a high-spin ferrous Fe_B antiferromagnetically (or ferromagnetically) coupled to a low-spin ferric heme b_3. The entire first reduction step is

dx.doi.org/10.1021/bi300496e | *Biochemistry* 2012, 51, 5173−5186

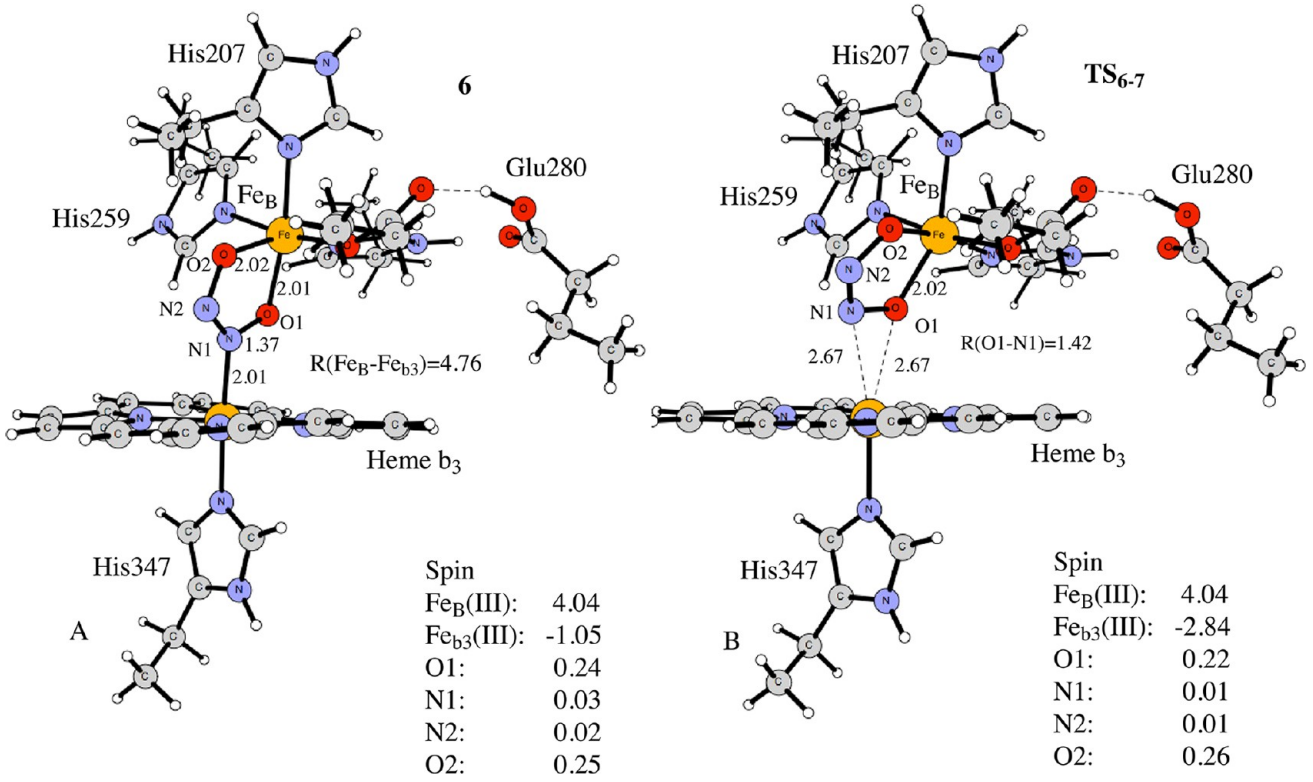

Figure 6. Optimized structures of (A) the *cis*-hyponitrite intermediate (**6**, quintet) and (B) the transition state for rotation of the hyponitrite ($\mathbf{TS_{6-7}}$, triplet). A few interatomic distances are given (in angstroms), as well as the most important spin populations.

calculated to be exergonic by 5.7 kcal/mol relative to the oxidized state with an oxo bridge, which is used as the reference in the energy diagram shown in Figure 3. The energy level of the singly reduced hydroxo state is fully determined by the restriction that the experimental exergonicity of the entire cycle should be reproduced, and is independent of the choice of the parameter for the cost of proton uptake discussed above.

The second proton affinity, yielding a water molecule at the BNC, is smaller than the first by 11.9 kcal/mol. This means that with the parametrization of the proton cost introduced above, making the first proton uptake endergonic by 3 kcal/mol, the second proton uptake is endergonic by 14.9 kcal/mol. The electron transfer is slightly endergonic, yielding a total endergonicity for the entire second reduction step of 16.4 kcal/mol. The large endergonicity of the second reduction step is in agreement with experimental indications that the reduction potential of heme b_3 is low and that heme b_3 therefore is more difficult to reduce than Fe_B.[15] At variance with the calculations and also with the previous experiment,[15] a more recent experiment indicates that the reduction potentials of the two iron centers are very similar.[16] Apparently, it is rather difficult to determine the reduction potential of Fe_B, and our calculations actually indicate that at least one of the assumptions used in the recent experiment[16] might not be fulfilled, namely that heme b_3 stays in the high-spin state when Fe_B becomes reduced. As mentioned above, when Fe_B is reduced, heme b_3 switches to a low-spin state (see Figure 1B). The optimized structure of the doubly reduced BNC with the water molecule still bound (**3**) is shown in Figure 4B. The ground state is a quintet with no spin on the low-spin ferrous heme b_3. The water molecule turns out to be bound by 3.4 kcal/mol, which makes the empty doubly reduced BNC (**4**) the highest point on the energy surface, yielding a total activation energy of 19.8 kcal/mol relative to the lowest previous point, which is also the largest activation energy in the entire catalytic cycle (see below). In the empty reduced BNC, the ferrous heme b_3 has an intermediate spin, which can be either antiferromagnetically or ferromagnetically coupled to the high-spin ferrous Fe_B (see Figure 5A). The calculated activation energy of 19.8 kcal/mol is somewhat too high, compared to the experimental value of 15.9 kcal/mol, obtained from the turnover rate of NOR in *Paracoccus denitrificans*[37] using transition state theory, but still within the uncertainty of the calculations. It should also be noted that it might not be necessary to fully release the water molecule before the first NO molecule enters, which could lower the barrier somewhat. Extensive calculations were performed to investigate such a scenario, but it was not possible to find a structure of that type with a lower energy, partly because of the difficulties in accurately determining the entropy for a state with two loosely bound molecules (water and NO). Another possibility is that the binding energy of the water molecule in the reduced BNC is overestimated by the B3LYP* functional, which is indicated by the fact that with the B3LYP functional the water molecule is essentially unbound. In fact, using the B3LYP functional, a lower value for the total barrier for this part of the energy profile is found, close to the experimental value of 16 kcal/mol. The lowering compared to the B3LYP* value is a result not only of the decreased water binding energy but also of a change in the relative reduction potentials of the two metal centers.

In the energy profile in Figure 3, the solid lines correspond to explicitly calculated values adjusted only to reproduce the experimental exergonicity of the entire catalytic cycle. As mentioned above, via the introduction of one parameter, the energetics of individual proton and electron transfer steps can also be calculated, and the corresponding energy levels are

dx.doi.org/10.1021/bi300496e | *Biochemistry* 2012, 51, 5173−5186

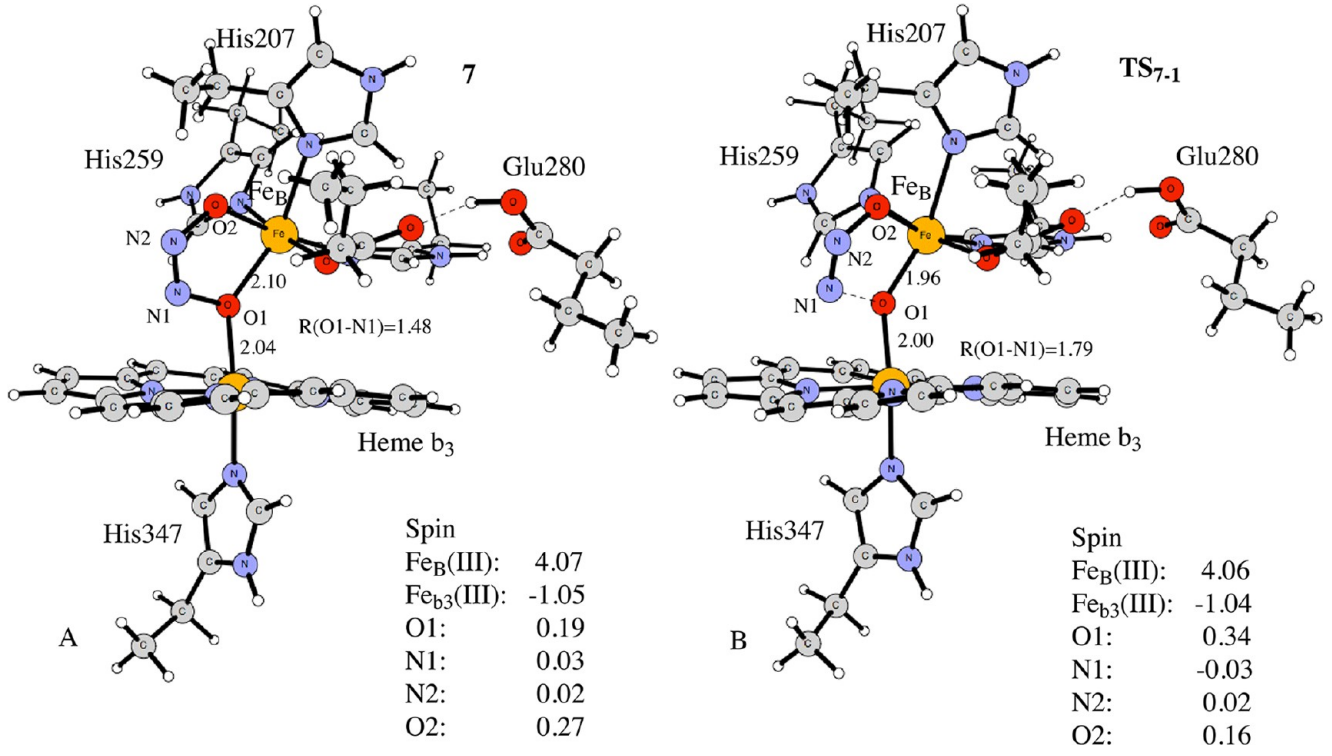

Figure 7. Optimized structures of (A) the intermediate with rotated hyponitrite (7, quintet) and (B) the transition state for N−O bond cleavage (TS_{7-1}, quintet). A few interatomic distances are given (in angstroms), as well as the most important spin populations.

shown as dashed curves in the energy profile to indicate that they are less well determined by the calculations than the rest of the diagram. In the same way, possible barriers for proton and electron transfer are shown as dashed lines in the energy profile. Obviously, those cannot be calculated using our model, and therefore, approximate values for these barriers are taken from experimental information. The barrier for the first proton transfer can be estimated from an experiment with fully reduced NOR to be discussed below[19] and is set to ∼14.5 kcal/mol. Because the second proton transfer is calculated to be endergonic by 14.9 kcal/mol with the present parametrization, there is no barrier apart from the endergonicity for this step, assuming that the barrier is the same as for the first proton transfer. The transfer of an electron from heme b to the BNC is assumed to be very fast, and therefore, the electron transfer barriers are indicated to be only a few kilocalories per mole in the energy diagram.

N−N Bond Formation. NO binds to the fully reduced BNC with a structure (**5**) shown in Figure 5B; i.e., it binds with the nitrogen to heme b_3 and with the oxygen coordinating to Fe_B. The ground state is a quartet, with a sextet state ∼2 kcal/mol higher in energy, and with a binding energy of 7.0 kcal/mol relative to the empty two-electron-reduced BNC (**4**). An alternative way to reach this point, which is 12.8 kcal/mol above the lowest previous point on the energy profile, would be to bind the NO molecule to the singly reduced BNC, which would increase the affinity for the second electron. However, one still has to pay the cost of the proton transfer (14.9 kcal/mol) and the release of the water molecule (bound by 4.4 kcal/mol to the singly reduced BNC). Furthermore, NO is unbound by 5.5 kcal/mol to the singly reduced BNC, and the NO molecule binds with nitrogen to the reduced Fe_B, which for the fully reduced BNC is an excited state (by 9.3 kcal/mol); a rotation of the NO molecule therefore has to occur. Taken together, this means that the barrier for reaching state **5** this way would be higher than the reaction path shown in Figure 3. When a second NO molecule approaches the BNC, the lowest-energy path is obtained by just letting the nitrogen of the second NO approach the nitrogen of the already bound NO. In this way, the N−N bond is formed with essentially no barrier at all, and the stable *cis*-hyponitrite (**6**) shown in Figure 6A is formed −10.3 kcal/mol below the initial oxo state. Thus, the barrier for the formation of this intermediate is determined by the position of the two-electron-reduced BNC (**4**). Both irons are now oxidized, and the ferric high-spin Fe_B can be either ferromagnetically or antiferromagnetically coupled to the ferric low-spin heme b_3. The spin populations (0.24 and 0.25) on the two oxygens of the hyponitrite dianion, both coordinated to Fe_B, are typical for ligands to high-spin ferric non-heme iron with a high degree of spin delocalization.

N−O Bond Cleavage. The most complicated part of the reaction path turned out to be the cleavage of the N−O bond starting from the stable hyponitrite intermediate **6**. Trying to just increase the N−O distance to form an oxo-group at Fe_B with N_2O coordinating to the heme b_3 iron, gave very high energies, making such a reaction path inaccessible. Instead it was found that if the hyponitrite is rotated in the BNC such that the Fe−N bond is cleaved and oxygen coordinates to both irons, see Figure 7A, then the N−O bond can be cleaved with a reasonable barrier. The transition state for rotation of the hyponitrite, labeled TS_{6-7} and shown in Figure 6B, has the same length for the Fe−N bond to be cleaved and the Fe−O bond to be formed, 2.67 Å, and the ferric heme iron has intermediate spin coupling, because of the long distance between the iron and the distal ligand. The calculated barrier for the rotation is 14.7 kcal/mol, significantly lower than the calculated barrier of 19.8 kcal/mol to reach the stable hyponitrite intermediate from oxidized state **1**, and in good

dx.doi.org/10.1021/bi300496e | *Biochemistry* 2012, 51, 5173−5186

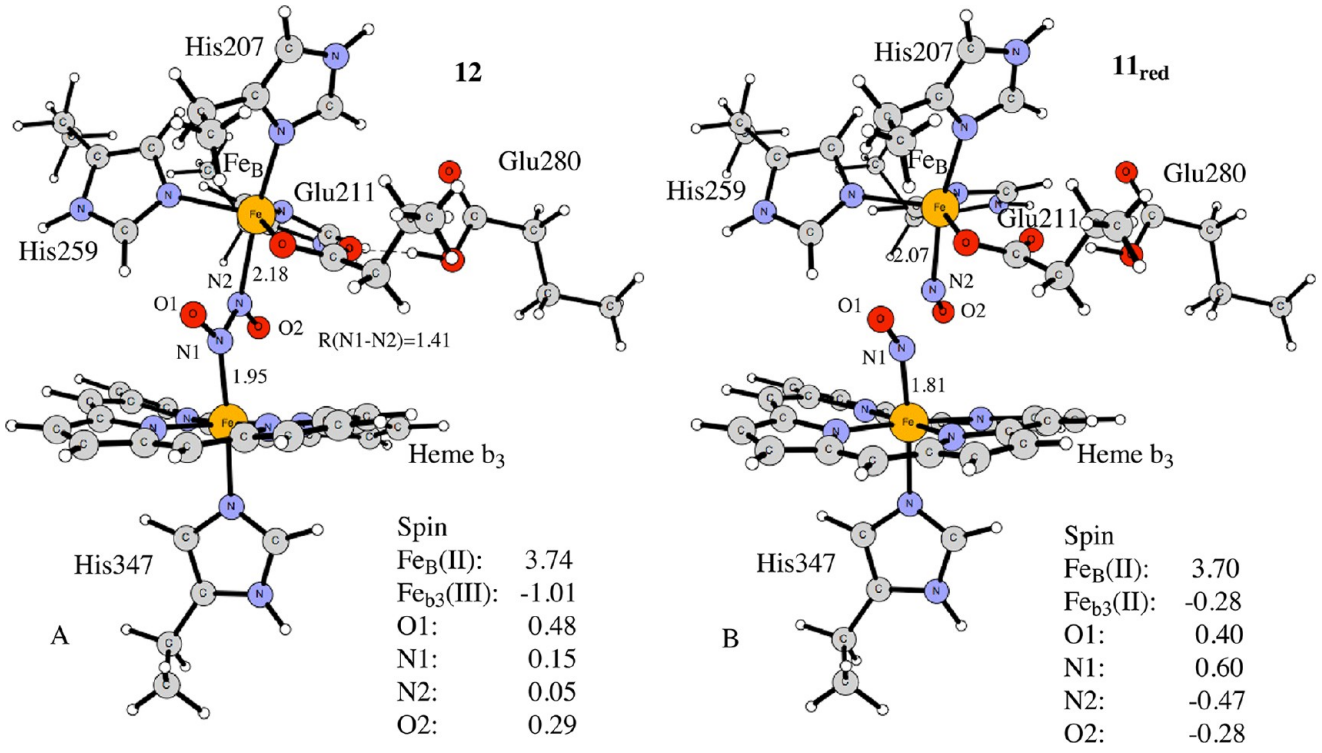

Figure 8. Optimized structures of (A) the *trans*-hyponitrite intermediate (**12**, quintet) and (B) the two-electron-reduced BNC with one NO bound to each Fe (labeled $\mathbf{11}_{red}$, quintet). A few interatomic distances are given (in angstroms), as well as the most important spin populations.

agreement with an experimental value of 13.3 kcal/mol estimated from an experiment on the fully reduced enzyme[12] (see below). The new intermediate with a rotated hyponitrite, **7**, is shown in Figure 7A, and it is 2.6 kcal/mol higher in energy than the originally formed hyponitrite, **6**. The length of the N−O bond to be cleaved in the next step has increased from 1.37 Å in **6** to 1.48 Å in **7**, and the barrier for cleaving this bond is 7.0 kcal/mol relative to the rotated hyponitrite intermediate, which means that it is 9.6 kcal/mol relative to the lowest previous point, **6**. The optimized transition state $\mathbf{TS}_{7-1}$ is shown in Figure 7B, and it leads directly to oxo intermediate **1** and free N_2O in a very exergonic step, ending at −38.4 kcal/mol relative to the starting point and thereby closing the catalytic cycle.

An important structural point to note here is that both *cis*-hyponitrite structures, **6** and **7**, have two bonds between Fe_B and the substrate, in contrast to the rest of the intermediates in the catalytic cycle, which have only one. Therefore, the Fe_B coordination has to change from a trigonal bipyramidal to an octahedral coordination when the *cis*-hyponitrites are formed. This structural change occurs essentially through a rotation of Glu211 such that only one of the carboxylate oxygens is left in the equatorial plane. The structural change turns out to be most important in intermediate **7**, which apparently has the strongest bonds between Fe_B and the substrate, and it leads to an energy decrease of 7 kcal/mol, while the energetic effect in **6** is <1 kcal/mol. Both transition states surrounding intermediate **7**, $\mathbf{TS}_{6-7}$ and $\mathbf{TS}_{7-1}$, are lowered by 3−4 kcal/mol by the structural change, i.e., approximately half the effect in **7**. It can be noted that in this model the rotation of the Glu211 carboxylate group does not occur automatically, because there is a small barrier involved, and therefore, calculations on a much smaller model were very helpful when searching for the optimal structure along this part of the reaction path. In transition state $\mathbf{TS}_{6-7}$, there is a second aspect to be noted, apart from the important change in the coordination structure of Fe_B. Because of the long distance between the heme iron and the distal ligands (2.67 Å), intermediate spin coupling at the heme iron was found to give an energy for the transition state lower than that for the low-spin coupling present in most of the intermediates of the catalytic cycle. With an antiferromagnetic coupling between the irons, this means that the spin state changes from a quintet to a triplet. At the B3LYP* level, this spin change lowers the barrier by ∼2 kcal/mol, giving a final value of 14.7 kcal/mol. At the B3LYP level, the effect is somewhat larger, as expected, giving a barrier of only 12.8 kcal/mol. The high-spin coupling at the heme iron, which is involved in oxo intermediate **1**, was found to have a higher energy for transition state $\mathbf{TS}_{6-7}$.

It can be noted that this part of the catalytic cycle, N−O bond cleavage, is somewhat different from that suggested in the previous study,[7] in which a ferryl intermediate was first formed when the N−O bond is cleaved. This difference between the two studies is probably caused by the water molecule coordinating to Fe_B in the model used in the previous study. The extra ligand makes the hyponitrite intermediate much less stable,[7] thereby making the N−O bond easier to cleave. In this study, we show that a water ligand at Fe_B would be unbound relative to bulk water. Furthermore, relative to the lowest previous intermediate (which is not the *cis*-hyponitrite in that study), the energy of the N−O bond cleavage was actually quite high (21.3 kcal/mol).

Trans Mechanisms. As mentioned in the introductory section, several authors have suggested a trans mechanism involving an intermediate in which a trans form of the hyponitrite is coordinated to the BNC with two Fe−N bonds, **12** in Figure 2.[1−3,5,9,13] Therefore, such a mechanism was also probed by calculating the relative energy of an intermediate

dx.doi.org/10.1021/bi300496e | *Biochemistry* 2012, 51, 5173−5186

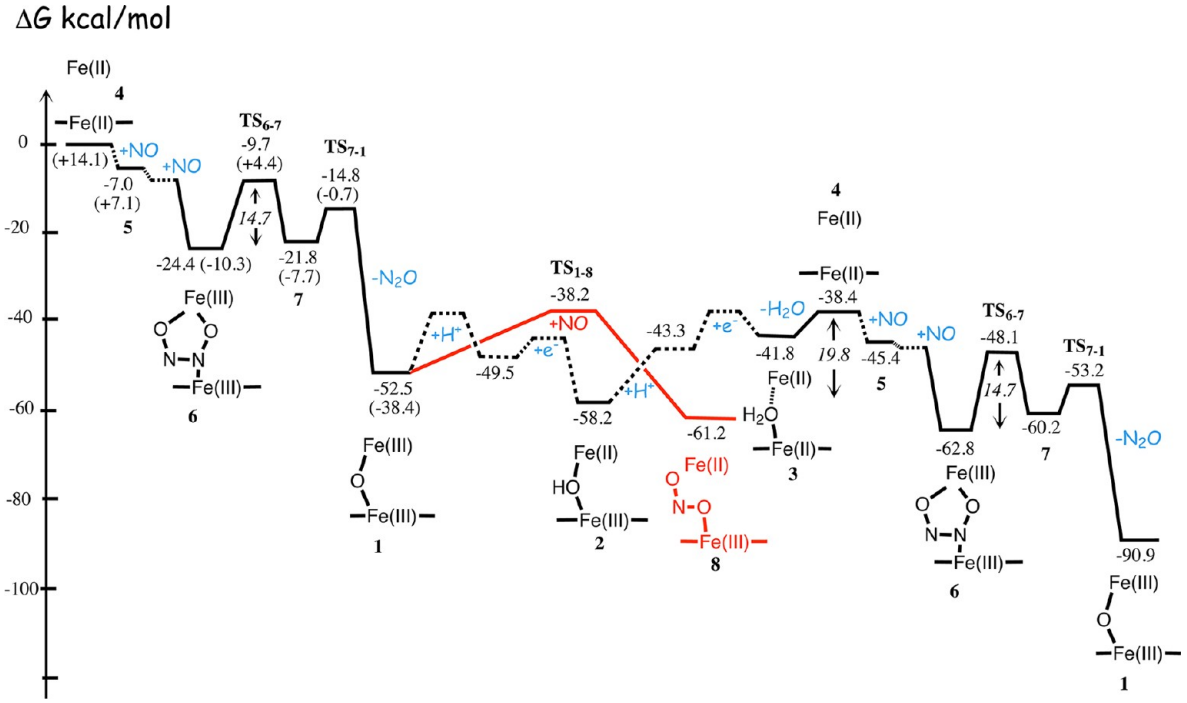

Figure 9. Calculated free energy profile for the two cycles of the four-electron-reduced NOR (black curve). In this diagram, **4** is used as a reference point for the relative energies. The numbers in parentheses refer to the energy values given in Figure 3, which used a different reference point (**1**). The red curve corresponds to a side reaction between oxidized NOR and NO leading to nitrite (see the text).

with a *trans*-hyponitrite. However, the optimized trans intermediate (**12**) (Figure 8A) was found to be very high in energy, 16.9 kcal/mol above the reference point for the energy in Figure 3, **1**, which means that it is 22.6 kcal/mol higher than the lowest previous point, **2**, on the energy surface. The high energy of this intermediate makes it unlikely to be involved in the reaction mechanism of NOR, and in particular, the low-energy reaction path from the doubly reduced BNC **4** to the *cis*-hyponitrite **6** makes it impossible to prevent the system from going to **6** rather than to **12**. The *cis*-hyponitrite **6** is found to be as much as 27.2 kcal/mol lower in energy than the *trans*-hyponitrite **12**. One reason for the high energy of the trans intermediate **12** is probably that Fe_B is still reduced and what is formed is a hyponitrite radical ion with a single negative charge (see Figure 8A). Apparently, without the stabilizing coordination between the positively charged Fe_B ion and the two oxygen atoms, which is present in the cis intermediate **6**, the transfer of an electron from the ferrous Fe_B to the hyponitrite is too unfavorable in the trans intermediate **12**. A similar effect is obtained if O2 in the *cis*-hyponitrite structure **6** in Figure 6A is rotated 180° around the N−N axis into a trans structure where the oxygen atom is no longer coordinating to Fe_B. As a result, the energy is increased by 12.9 kcal/mol, the spin on the hyponitrite is increased, and Fe_B reaches an oxidation state intermediate between ferrous and ferric. A possible stabilization of the *trans*-hyponitrite structure **12** via addition of a water molecule was also tried, making the Fe_B six-coordinate and thereby promoting the transfer of an electron from Fe_B. A slightly increased level of electron transfer was indeed observed; however, the water ligand was not bound relative to bulk water, and no stabilization of the trans intermediate was therefore obtained.

Experiments with the Fully Reduced Enzyme. As mentioned in the introductory section, the NOR enzyme can be prepared in a fully reduced form, with all four metal cofactors reduced, which allows the study of two turnovers of the NO reduction reaction according to eq 1. In a recent study, the "flow-flash" technique was used to follow the reaction of the four-electron-reduced NOR from *Pa. denitrificans*,[19] and several results from that study can be compared to the energetics calculated here. To simplify this comparison, we have drawn a new energy profile (Figure 9), in which the empty two-electron-reduced BNC, which is the starting point for the NO reduction in the experiment, is used as the reference point for the energy. Furthermore, the energy diagram is extended to cover the full reaction that the four-electron reduced enzyme is capable of performing. The experiment shows that the reaction of the reduced BNC with NO is fast (1 μs), which is in agreement with the essentially barrierless binding of NO to the two-electron-reduced BNC obtained in the calculations, i.e., going from **4** via **5** to **6** in the energy profile in Figure 9, where a possible barrier due to the entropy loss during the NO binding process is ignored. The experiment furthermore shows that the first NO turnover, producing the first N_2O, occurs without the uptake of protons, and it was concluded that the protons must be taken up internally from the protein.[19] The mechanistic scenario proposed here is in agreement with the experimental observation but gives a different explanation, namely that no protons are needed for the production of the first N_2O, going from **4** to **1** in the energy profile in Figure 9.

In the flow-flash experiment, the uptake of protons from solution was observed on the same time scale as the oxidation of the low-spin hemes (heme b and heme c),[19] which is also in accordance with the mechanistic scheme in Figure 9, where the reduction of the BNC in both the step from **1** to **2** and the step from **2** to **3** is coupled to proton uptake. The rate constant for the first low-spin heme oxidation was found to be 50−120 s^{-1}, depending on the NO concentration,[19] which corresponds to a barrier of 14.6−15.1 kcal/mol using transition state theory. Furthermore, the rate of this reaction step was found to be pH-

dx.doi.org/10.1021/bi300496e | *Biochemistry* 2012, 51, 5173−5186

dependent, decreasing the barrier by 0.6−0.8 kcal/mol when the pH was decreased from 7.5 to 6.0. These observations imply that the rate-limiting step for the first oxidation to occur is the uptake of the proton by the oxo bridge in **1**, which was also mentioned above to be used here to set an approximate barrier for the proton transfer step of 14.5 kcal/mol. These experimental observations also indicate that the barrier for N−O bond cleavage is lower than the barrier for the first oxidation step, i.e., lower than ∼14 kcal/mol. A similar conclusion was reached in a previous study of the fully reduced enzyme, indicating that the first turnover occurs with a rate constant of 1000 s^{-1}, corresponding to a barrier of 13.3 kcal/mol.[12] On the calculated energy profile, the rate-limiting transition state for N−O bond cleavage, when starting from the reduced BNC **4**, is $\mathbf{TS_{6-7}}$, the rotation of hyponitrite, corresponding to a barrier of 14.7 kcal/mol, thus in good agreement with the experimental observations, considering the uncertainty in the calculations.

Experimentally, the second step of low-spin heme oxidation was found to be slower than the first, with rate constants of 3−12 s^{-1}, depending on the NO concentration.[19] These rates correspond to a barrier of 16.0−16.8 kcal/mol, which is also in agreement with the turnover rate of the enzyme[37] mentioned above, corresponding to an overall barrier of 15.9 kcal/mol. In the calculations, the second reduction of the BNC (**2** to **3**) is found to be endergonic by 16.4 kcal/mol (including both proton and electron transfer), very close to the experimental barrier. However, for this reduction step to occur, it has to be followed by water release and NO binding to reach, in the first instance, the low-lying hyponitrite compound **6**, and eventually the final product **1**. This adds up to a calculated barrier of 19.8 kcal/mol for the second reduction step. Thus, the calculations agree with the experimental observation that the rate for the second reduction of the BNC is slower than the first one, even if the calculated barrier is 3−4 kcal/mol too high. As already mentioned above, one explanation for the high calculated barrier could be that the first NO molecule actually starts to bind to the BNC before the water molecule is fully released, a situation that cannot be easily described by the calculations. Another possibility is that there is an error in the calculated relative reduction potentials for the two iron centers, which is indicated by the large difference in electron affinity between Fe_B and the heme iron obtained in the calculations, 10.2 kcal/mol, while the experimental reduction potentials correspond to a difference of 6.0 kcal/mol[15] or are even found to be isopotential[16] (see also above). Either the electron affinity of the ferric heme iron should be larger, or the electron affinity of Fe_B should be lower. A correction of such an error would in either case shift the energy of **2** to a higher level and thereby decrease the barrier for the entire second reduction step. It is interesting to note that a similar problem was encountered in a computational study of the catalytic cycle of cytochrome *c* oxidase, in which the calculated exergonicity of reduction of ferric heme was found to be too low compared to those of the other reduction steps, and a correction was introduced to improve the shape of the energy profile.[38] As mentioned above, using the B3LYP functional instead of the B3LYP* functional gives a lower barrier for the second reduction step, indicating a sensitivity to the functional. Finally, in the experiment, the second low-spin heme oxidation step was also found to be sensitive to pH, decreasing the barrier by 0.3−1.3 kcal/mol when the pH was decreased from 7.5 to 6.0.[19] This is in agreement with the calculated energy profile in Figure 9, where the endergonic uptake of the proton by the bridging hydroxide **2** is part of the barrier for the second reduction of the BNC.

In another experimental study, an NO-saturated solution was mixed with the fully reduced NOR from *P. aeruginosa*, and the EPR spectrum obtained was interpreted to show that two molecules of NO were bound to the BNC, one to the ferrous Fe_B and one to the pentacoordinate ferrous heme b_3;[5] this was suggested to be an intermediate during the catalytic reaction.[5,13] Calculations were performed to investigate such a structure, but it was rather difficult to obtain a structure in which the N−N bond was not already formed. One such structure was eventually found, shown in Figure 8B (labeled $\mathbf{11}_{red}$ because it is one-electron-reduced compared to **11** in mechanism II in Figure 2), but it is 8.2 kcal/mol higher in energy than the reduced starting point of the experiment, **4**, and should therefore not be observable. Thus, the calculations indicate that the EPR signals observed do not correspond to an intermediate in the catalytic cycle for NO reduction. In the same study, it was also found that after the completion of the NO reaction with the fully reduced NOR an EPR signal corresponding to a ferric high-spin heme b_3 could be observed, in contrast to the EPR silent oxidized resting state.[5] It was therefore concluded that the fully oxidized BNC with an oxo brigde is not part of the catalytic cycle during turnover, and a mechanism with an empty oxidized BNC was suggested.[5,13] This is in contrast to our calculations, which definitely show that the diferric state with an oxygen bridge is involved in the catalytic cycle of NO reduction. A likely explanation for the observed high-spin heme b_3 EPR signal in the final product of the single-turnover cycle[5] is that the oxidized BNC with an oxo bridge undergoes some further reactions, possibly with remaining NO molecules in the saturated buffer, finally resulting in an empty BNC with an oxidized high-spin heme b_3 (see below). Such a form of the BNC would, however, not be involved in the normal catalytic cycle of the enzyme.

NO Binding to Oxidized NOR and Substrate Inhibition. Bacterial NOR is known to exhibit substrate inhibition during steady state turnover[1] with a maximal activity for micromolar NO concentrations. In the flow-flash study discussed above, it was shown for the first time that substrate inhibition occurs during a single oxidative cycle.[19] It was found that the rate of oxidation of the low-spin hemes depends on the NO concentration, with higher rates for 75 μM NO than for 1.5 mM NO; i.e., an overly high concentration of NO inhibits the reduction of the BNC. It was furthermore found that the substrate inhibition was stronger for pH 6.0 than for pH 7.5.[19] It has also been observed in several studies that NO binds to oxidized NOR,[14,39] and it has therefore been natural to suggest that the cause of the substrate inhibition is that NO binds to the oxidized BNC.[1,19] However, there is no specific mechanism suggested for how NO bound to the oxidized BNC could lead to substrate inhibition. The calculations indicate that a very weak complex might be formed between NO and the oxidized BNC with the oxo bridge still present. Such a complex could be photolabile, as observed,[14] but in contrast to the suggestion based on the experimental observations that NO binds to heme b_3 in the oxidized BNC,[14] the calculations indicate that the most likely site for NO binding is Fe_B, which then becomes six-coordinated with the oxo bridge still present. As noted in ref 14, the observed Fe−NO stretch frequency actually also fits well with previously observed frequencies for non-heme NO complexes. More interestingly, the calculations also show that NO can react quite readily with the oxo bridge in the oxidized

dx.doi.org/10.1021/bi300496e | *Biochemistry* 2012, 51, 5173−5186

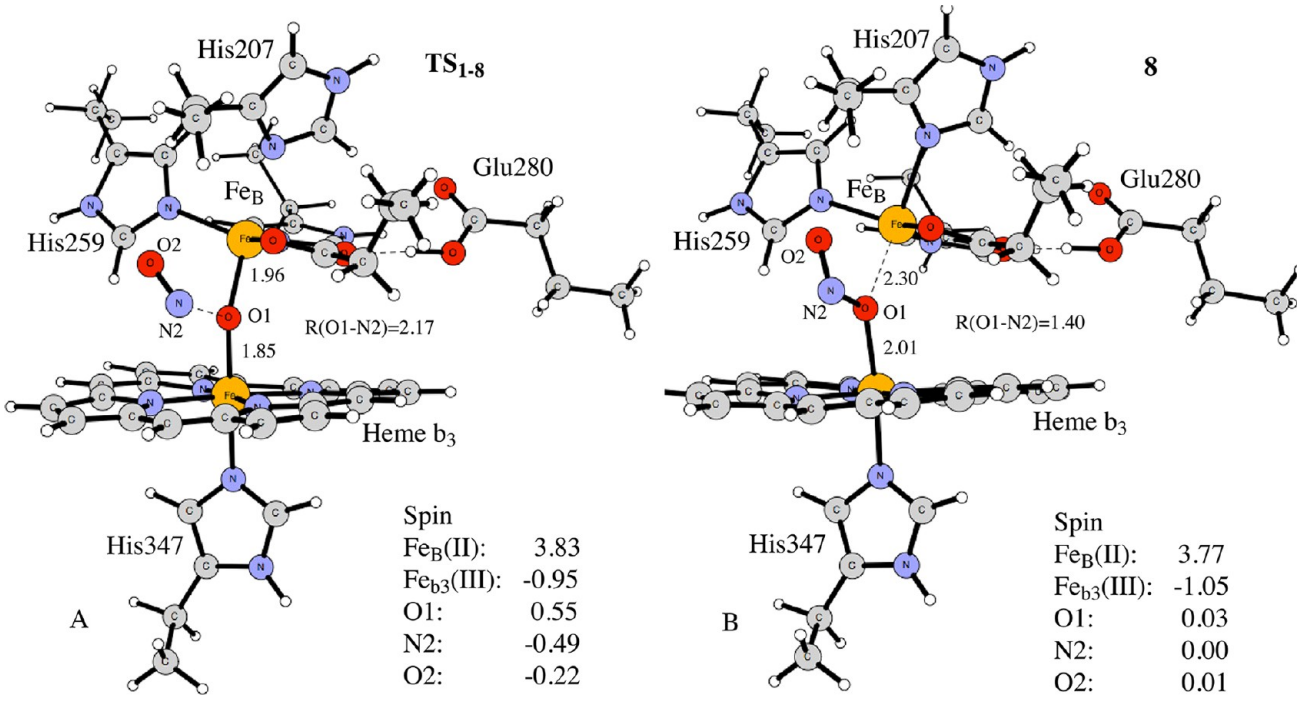

Figure 10. Optimized structures for (A) the transition state for nitrite formation from the oxidized intermediate **1** ($\mathbf{TS_{1-8}}$, quartet) and (B) the nitrite product (**8**, quartet). A few interatomic distances are given (in angstroms), as well as the most important spin populations.

BNC, **1**, to form a nitrite molecule, NO_2^-. The calculated barrier for the reaction is 14.3 kcal/mol, and the exergonicity for this reaction step is 8.7 kcal/mol (red curve in Figures 3 and 9). The low barrier can be explained by the radical character of the oxygen in the oxo bridge, which easily reacts with the radical NO. The optimized transition state, $\mathbf{TS_{1-8}}$, is shown in Figure 10A and the nitrite product **8** in Figure 10B, where it can be seen that Fe_B is reduced to the ferrous form by an electron from the substrate. Interestingly, in one of the experimental studies of the NO reaction with oxidized NOR, it is noted that the observed spectrum suggests the presence of a fraction of reduced low-spin hemes in the NO-bound complexes,[39] which might indicate an equilibration of the electron in Fe_B (see below). It should be mentioned that the reaction of NO with a hydroxo bridge in the oxidized BNC does not lead to a stable product and is therefore less likely.

Nitrite formation by the reaction of NO with the oxo bridge in the BNC is thus one plausible explanation for the observed reaction between NO and the oxidized NOR. It is possible that a weakly bound photolabile NO complex might also be observable and spectroscopically characterized, but such a complex cannot explain the substrate inhibition. Nitrite formation, on the other hand, can explain the observed deceleration of the catalytic reaction rate at higher NO concentrations if it is noted that the barrier for this side reaction is similar in height to the barrier for the forward catalytic reaction (see Figure 9), and if it is considered that the transition state $\mathbf{TS_{1-8}}$ will be lowered at higher NO concentrations because of an increased entropy contribution. Thus, with a lower barrier for nitrite formation at high NO concentrations, this side reaction will compete with the forward catalytic reaction. Because the catalytic reaction after several steps is more exergonic than the side reaction (see Figure 9), the nitrite product **8** will eventually go back to **1** and then continue forward to the final product, but with a slower rate because **8** is lower in energy than both **1** and **2**, making the barriers higher for both reduction steps. It should be noted, though, that, even if the energy diagram in Figure 9 can give a simplified mechanism for the observed substrate inhibition, it cannot give a detailed description of substrate inhibition, indicating that the real situation is more complicated. For example, the experiments indicate that the substrate inhibition is stronger at low pH,[19] which could be explained if protonation of the nitrite would stabilize the nitrite product of the side reaction and thus further increase the barriers for the forward reaction steps, and if such a protonation was possible only at lower pH. However, the calculations indicate that the proton affinity of the nitrite is too low to support such an explanation.

This seems to be the first time that nitrite formation is suggested to occur in the reaction between NO and oxidized NOR. However, it has previously been shown that one possible mechanism for NO inhibition in cytochrome *c* oxidase is the formation of nitrite in the reaction between NO and oxidized cytochrome *c* oxidase, and that this reaction is coupled to reduction of the low-spin heme.[40,41]

Modifications of the Mechanism. The different mechanisms that have been suggested for the catalytic NO reduction in NOR are normally classified as trans or cis mechanisms, depending on whether a *trans*- or *cis*-hyponitrite is involved as an intermediate (see Figure 2). As discussed above, the model calculations presented here strongly disfavor a trans mechanism on an energy basis and instead present a likely cis:b_3 mechanism. However, there are also other differences between the two mechanisms presented in Figure 2 that deserve to be investigated. One difference concerns whether NO binds to the BNC before or after the second electron enters, which was discussed above. The calculations indicate that the total barrier for the second reduction of the BNC would be higher if NO enters into the singly reduced BNC; therefore, it is most likely that NO enters into the two-electron-reduced BNC, as suggested in mechanism I in Figure 2. Another difference between the two mechanisms concerns whether protons enter

dx.doi.org/10.1021/bi300496e | *Biochemistry* 2012, 51, 5173−5186

the BNC before the N−O bond is cleaved (compare the step from **6** to **1** in mechanism I in Figure 2 with the step from **12** to **13** in mechanism II). Partly connected to this protonation issue is the question of whether the fully oxidized BNC has an oxo bridge during turnover (compare intermediates **1** and **9** in Figure 2). The calculations have shown that it is possible to cleave the N−O bond with a reasonable barrier without protonation of the *cis*-hyponitrite (see Figure 3 or 9). However, the possibility that the barrier would be even lower for a process in which the hyponitrite is protonated before the N−O bond cleavage cannot be excluded. The proton affinity of the *cis*-hyponitrite structure **6** is calculated to be ∼14 kcal/mol lower than that of the singly reduced hydroxo intermediate **2**, which was already very low. On the other hand, it was also found that in the protonated *cis*-hyponitrite the N−O bond can be cleaved with essentially no extra barrier. The barrier for the N−O bond cleavage in the protonated hyponitrite is therefore determined by the cost of the uptake of a proton from the bulk and can therefore not be definitely determined from the calculations because it depends on the parametrization. However, considering the very low proton affinity of the hyponitrite, it is not likely that the barrier for protonation of the hyponitrite is lower than the barrier for N−O bond cleavage in the unprotonated hyponitrite, which was calculated to be 14.7 kcal/mol. Furthermore, after an N−O bond cleavage in the protonated hyponitrite, the N_2O molecule formed is strongly unbound and would leave the BNC with a fairly stable diferric hydroxo-bridged BNC. The uptake of a second proton by the fully oxidized and already protonated BNC, needed to form a water molecule that could leave, would be considerably more endergonic than the first. Therefore, the formation of an empty oxidized BNC without an oxygen ligand during the catalytic turnover is extremely unlikely. Thus, an unlikely but not impossible alternative to the oxo bridge in the oxidized BNC is a hydroxy bridge, while the possibility of an empty BNC seems to be excluded. In a scenario with protonation of the hyponitrite before N−O bond cleavage, the first reduction of the BNC can occur at different stages, either before the N−O bond cleavage or after it, and with electrons available, the product of the N−O bond cleavage would be the singly reduced BNC with a hydroxo ligand **2**, i.e., the same as in the mechanism suggested here (with electrons available).

SUMMARY AND CONCLUSIONS

A model of the diiron active site (BNC) in NO reductase was built on the basis of the first crystal structure of NOR published in 2010[10] and used in hybrid density functional theory calculations to explore the mechanisms of the catalytic reaction, the two-electron reduction of nitric oxide to produce nitrous oxide and water. The calculations result in a free energy profile that agrees well with experimental information and suggests a catalytic mechanism of the so-called cis:b_3 type (see Figures 3 and 9). The fully oxidized state with an oxo bridge (**1**) is reduced and protonated twice to eliminate a water molecule and to form the empty diferrous BNC (**4**) that can react with NO. The first reduction step is found to be exergonic and the second one endergonic, as is the release of the water molecule. Both the first and second molecules of NO, on the other hand, are exergonically bound to the reduced BNC, with essentially no extra barrier on top of the endergonic reduction. The product is a dianionic *cis*-hyponitrite, coordinating to two ferric irons in a quite stable intermediate (**6**), calculated to be 10.3 kcal/mol more stable than the initial oxidized state (**1**). The highest point on this part of the energy profile is the empty reduced BNC (**4**), 14.1 kcal/mol above the initial oxidized state and 19.8 kcal/mol above the lowest previous point (the singly reduced and protonated BNC, **2**). Thus, the barrier for formation of the *cis*-hyponitrite intermediate starting with the oxidized BNC is calculated to be 19.8 kcal/mol, which is 4 kcal/mol higher than the value of ∼16 kcal/mol obtained from experimental estimates.[19,37] Considering the expected uncertainty in this type of calculation, this should be considered as a satisfactory agreement between experiment and theory. Possible sources of error are discussed in the text.

After reduction of the BNC and the formation of the N−N bond described in the previous paragraph, one of the N−O bonds should be cleaved to form the product N_2O. This is found to occur in a quite exergonic reaction step, resulting in the oxo-bridged diferric BNC (**1**) and a free N_2O. The calculated barrier of 14.7 kcal/mol ($\mathbf{TS_{6-7}}$) is in good agreement with experimental estimates of 13.3 kcal/mol for this reaction step.[12] During this reaction step, a structural rearrangement at the Fe_B is found to occur and to be energetically important. It is furthermore shown that the formation of a *trans*-hyponitrite intermediate is energetically much less favorable than the formation of a *cis*-hyponitrite, indicating that the so-called trans mechanism for the catalytic reaction in NOR can be discarded. Finally, it is shown that the oxo bridge in the fully oxidized state (**1**) can react with NO to form nitrite (**8**), explaning the experimentally observed reaction of the oxidized enzyme with NO, and possibly also the observed substrate inhibition at higher NO concentrations.

To obtain the energy profile for the entire catalytic cycle, we adjusted the calculated energetics of the reduction steps to reproduce the overall exergonicity of the catalytic reaction obtained from experimental reduction potentials. This gives a higher accuracy than if calculated absolute reduction potentials and pK_a values of donors and acceptors would be used. Comparing calculated relative reduction potentials and pK_a values of the same site (such as comparing the two reduction steps of the BNC) is more reliable than comparing values of different sites having different surroundings [such as comparing the donor sites (heme b and bulk water) with the acceptor sites (different parts of the BNC)]. The same procedure has been used in investigations of other similar reactions in which electrons and protons enter or leave, such as cell respiration and photosynthesis.[34,35]

ASSOCIATED CONTENT

Supporting Information

Cartesian coordinates for the most important structures. This material is available free of charge via the Internet at http://pubs.acs.org.

AUTHOR INFORMATION

Corresponding Author

*E-mail: mb@fysik.su.se. Phone: +46-8-16 12 64.

Notes

The authors declare no competing financial interest.

REFERENCES

(1) Girsch, P., and de Vries, S. (1997) Purification and initial kinetic and spectroscopic characterization of NO reductase from *Paracoccus denitrificans*. *Biochim. Biophys. Acta 1318*, 202−216.

(2) Moënne-Loccoz, P., and de Vries, S. (1998) Structural Characterization of the Catalytic High-Spin Heme b of Nitric Oxide

Reductase: A Resonance Raman Study. *J. Am. Chem. Soc. 120*, 5147−5152.
(3) Moënne-Loccoz, P., Richter, O.-M. H., Huang, H., Wasser, I. M., Ghiladi, R. A., Karlin, K. D., and de Vries, S. (2000) Nitric Oxide Reductase from *Paracoccus denitrificans* Contains an Oxo-Bridged Heme/Non-Heme Diiron Center. *J. Am. Chem. Soc. 122*, 9344−9345.
(4) Pinakoulaki, E., Stavrakis, S., Urbani, A., and Varotsis, C. (2002) Resonance Raman Detection of a Ferrous Five-Coordinate Nitrosylheme b_3 Complex in Cytochrome cbb_3 Oxidase from *Pseudomonas stutzeri*. *J. Am. Chem. Soc. 124*, 9378−9379.
(5) Kumita, H., Matsuura, K., Hino, T., Takahashi, S., Hori, H., Fukumori, Y., Morisima, I., and Shiro, Y. (2004) NO Reduction by Nitric-oxide Reductase from Denitrifying Bacterium *Pseudomonas aeruginosa*. *J. Biol. Chem. 279*, 55247−55254.
(6) Blomberg, L. M., Blomberg, M. R. A., and Siegbahn, P. E. M. (2006) A Theoretical Study on Nitric Oxide Reductase Activity in a ba_3-type Heme-Copper Oxidase. *Biochim. Biophys. Acta 1757*, 31−46.
(7) Blomberg, L. M., Blomberg, M. R. A., and Siegbahn, P. E. M. (2006) Reduction of Nitric Oxide in Bacterial Nitric Oxide Reductase: A Theoretical Model Study. *Biochim. Biophys. Acta 1757*, 240−252.
(8) Moënne-Loccoz, P. (2007) Spectroscopic characterization of heme iron-nitrosyl species and their role in NO reductase mechanisms in diiron proteins. *Nat. Prod. Rep. 24*, 610−620.
(9) Watmough, N., Field, S. J., Hughes, R. J. L., and Richardson, D. J. (2009) The bacterial respiratory nitric oxide reductase. *Biochem. Soc. Trans. 37*, 392−399.
(10) Hino, T., Matsumoto, Y., Nagano, S., Sugimoto, H., Fukumori, Y., Murata, T., Iwata, S., and Shiro, Y. (2010) Structural Basis of Biological N_2O Generation by Bacterial Nitric Oxide Reductase. *Science 330*, 1666−1670.
(11) Shapleigh, J. P., and Payne, W. J. (1985) Nitric oxide-dependent proton translocation in various denitrifiers. *J. Bacteriol. 163*, 837−840.
(12) Hendriks, J. H., Jasitis, A., Saraste, M., and Verkhovski, M. I. (2002) Proton and electron pathways in the bacterial nitric oxide reductase. *Biochemistry 41*, 2331−2340.
(13) Hino, T., Nagano, S., Sugimoto, H., Tosha, T., and Shiro, Y. (2012) Molecular structure and function of bacterial nitric oxide reductase. *Biochim. Biophys. Acta 1817*, 680−687.
(14) Pinakoulaki, E., Gemeinhardt, S., Saraste, M., and Varotsis, C. (2002) Nitric-oxide Reductase, Structure and Properties of the catalytic site from resonance raman scattering. *J. Biol. Chem. 277*, 23407−23413.
(15) Grönberg, K. L. C., Roldan, M. D., Prior, L., Butland, G., Cheessman, M. R., Richardson, D. J., Spiro, S., Thomson, A. J., and Watmough, N. J. (1999) A low redox potential heme in the dinuclear center of bacterial nitric oxide reductase: Implications for the evolution of energy-conserving heme-copper oxidases. *Biochemistry 38*, 13780−13786.
(16) Field, S. J., Roldan, M. D., Marritt, S. J., Butt, J. N., Richardson, D. J., and Watmough, N. J. (2011) Electron transfer to the active site of the bacterial nitric oxide reductase is controlled by ligand binding to heme b_3. *Biochim. Biophys. Acta 1807*, 451−457.
(17) Reimann, J., Flock, U., Lepp, H., Honigmann, A., and Ädelroth, P. (2007) A pathway for protons in nitric oxide reductase from *Paracoccus denitrificans*. *Biochim. Biophys. Acta 1767*, 362−373.
(18) Flock, U., Lachmann, P., Reimann, J., Watmough, N. J., and Ädelroth, P. (2009) Exploring the terminal region of the proton pathway in the bacterial nitric oxide reductase. *J. Inorg. Biochem. 103*, 845−850.
(19) Lachmann, P., Huang, Y., Reimann, J., Flock, U., and Ädelroth, P. (2010) Substrate control of internal electron transfer in bacterial nitric oxide reductase. *J. Biol. Chem. 285*, 25531−25537.
(20) Butland, G., Spiro, S., Watmough, N. J., and Richardson, D. J. (2001) Two conserved glutamates in the bacterial nitric oxide reductase are essential for activity but not assembly of the enzyme. *J. Bacteriol. 183*, 189−199.
(21) Zumft, W. G. (2005) Nitric oxide reductase of prokaryotes with emphasis on the respiratory heme-copper oxidase type. *J. Inorg. Biochem. 99*, 194−215.
(22) Noodleman, L., and Case, D. A. (1992) Density-Functional Theory of Spin Polarization and Spin Coupling in Iron−Sulfur Clusters. *Adv. Inorg. Chem. 38*, 423−470.
(23) Becke, A. D. (1993) Density-functional thermochemistry. III. The role of exact exchange. *J. Chem. Phys. 98*, 5648−5652.
(24) Reiher, M., Salomon, O., and Hess, B. A. (2001) Reparameterization of hybrid functionals based on energy differences of states of different multiplicity. *Theor. Chem. Acc. 107*, 48−55.
(25) *Jaguar*, version 7.6 (2009) Schrödinger, LLC, New York.
(26) Schwabe, T., and Grimme, S. (2007) Double-hybrid density functionals with long-range dispersion corrections: Higher accuracy and extended applicability. *Phys. Chem. Chem. Phys. 9*, 3397−3406.
(27) Siegbahn, P. E. M., Blomberg, M. R. A., and Chen, S.-L. (2010) Significant van der Waals Effects in Transition Metal Complexes. *J. Chem. Theory Comput. 6*, 2040−2044.
(28) Blomberg, M. R. A., Siegbahn, P. E. M., and Babcock, G. T. (1998) Modeling electron transfer in biochemistry: A quantum chemical study of charge separation in *Rhodobacter sphaeroides* and photosystem II. *J. Am. Chem. Soc. 120*, 8812−8824.
(29) Curtiss, L. A., Raghavachari, K., Redfern, R. C., and Pople, J. A. (2000) Assessment of Gaussian-3 and density functional theories for a larger experimental test set. *J. Chem. Phys. 112*, 7374−83.
(30) Siegbahn, P. E. M., and Blomberg, M. R. A. (1999) Density Functional Theory of Biologically Relevant Metal Centers. *Annu. Rev. Phys. Chem. 50*, 221−249.
(31) *Gaussian 03*, revision B.03 (2003) Gaussian Inc., Pittsburgh, PA.
(32) Siegbahn, P. E. M., Blomberg, M. R. A., and Blomberg, M. L. (2003) A Theoretical Study of the Energetics of Proton Pumping and Oxygen Reduction in Cytochrome Oxidase. *J. Phys. Chem. B 107*, 10946−10955.
(33) Blomberg, M. R. A., and Siegbahn, P. E. M. (2006) Quantum Chemistry Applied to the Mechanisms of Transition Metal Containing Enzymes: Cytochrome c Oxidase a Particularly Challenging Case. *J. Comput. Chem. 27*, 1373−1384.
(34) Siegbahn, P. E. M., and Blomberg, M. R. A. (2008) Modeling of Mechanisms for Metalloenzymes Where Protons and Electrons Enter or Leave. In *Computational Modeling for Homogeneous Catalysis and Biocatalysis* (Morokuma, K., and Musaev, J., Eds.) pp 57−81, Wiley-VCH, Weinheim, Germany.
(35) Siegbahn, P. E. M., and Blomberg, M. R. A. (2010) Quantum chemical studies of proton-coupled electron transfer in metalloenzymes. *Chem. Rev. 110*, 7040−7061.
(36) Yano, J., Kern, J., Irrgang, K.-D., Latimer, M. J., Bergmann, U., Glatzel, P., Pushkar, Y., Biesiadka, J., Loll, B., Sauer, K., Messinger, J., Zouni, A., and Yachandra, V. K. (2005) X-ray damage to the Mn_4Ca complex in single crystals of photosystem II: A case study for metalloprotein crystallography. *Proc. Natl. Acad. Sci. U.S.A. 102*, 12047−12052.
(37) Forte, E., Urbani, A., Saraste, M., Sarti, P., Brunori, M., and Guffre, A. (2001) The cytochrome cbb_3 from *Pseudomonas stutzeri* displays nitric oxide reductase activity. *Eur. J. Biochem. 268*, 6486−6490.
(38) Siegbahn, P. E. M., and Blomberg, M. R. A. (2009) The Combined Picture from Theory and Experiments on Water Oxidation, Oxygen Reduction and Proton Pumping. *Dalton Trans.*, 5832−5840.
(39) Kapetanaki, S. M., Field, S. J., Hughes, R. J. L., Watmough, N. J., Liebl, U., and Vos, M. H. (2008) Ultrafast ligand binding dynamics in the active site of native bacterial nitric oxide reductase. *Biochim. Biophys. Acta 1777*, 919−924.
(40) Sarti, P., Guffre, A., Forte, E., Mastronicola, D., Barone, M. C., and Brunori, M. (2000) Nitric oxide and cytochrome c oxidase: Mechanisms of inhibition and NO degradation. *Biochem. Biophys. Res. Commun. 274*, 183−187.
(41) Sarti, P., Forte, E., Mastronicola, D., Guffre, A., and Arese, M. (2012) Cytochrome c oxidase and nitric oxide in action: Molecular mechanisms and pathophysiological implications. *Biochim. Biophys. Acta 1817*, 610−619.